Supplementary Information

On the failure load and mechanism of polycrystalline graphene by nanoindentation

Z. D. Sha[1], Q. Wan[2], Q. X. Pei[3], S. S. Quek[3], Z. S. Liu[1,*], Y. W. Zhang[3,*] & V.B. Shenoy[4,5,*]

[1] International Center for Applied Mechanics, State Key Laboratory for Strength and Vibration of Mechanical Structures, Xi'an Jiaotong University, Xi'an 710049, China.

[2] Institute of System engineering, China Academy of Engineering Physics, SiChuan, MianYang, 621900, China

[3] Institute of High Performance Computing, A*Star, 138632, Singapore.

[4] Department of Materials Science and Engineering, University of Pennsylvania, Philadelphia, PA 19104, USA.

[5] Department of Mechanical Engineering and Applied Mechanics, University of Pennsylvania, Philadelphia, Pennsylvania 19104, USA.

Correspondence and requests for materials should be addressed to Z. S. (email: zishunliu@mail.xjtu.edu.cn), Y.W. (email: zhangyw@ihpc.a-star.edu.sg), and V.B. (email: vshenoy@seas.upenn.edu)

Molecular dynamics simulations

Molecular dynamics (MD) simulations are performed using the large-scale atomic/molecular massively parallel simulator (LAMMPS) code[1]. The adaptive intermolecular reactive empirical bond order (AIREBO) potential[2] is used to describe the interatomic interaction for tip and polycrystalline graphene. It should be noted that the smaller cutoff distance in the switching function of AIREBO potential should be taken in the range of 1.92−2.0 Å to avoid a known nonphysical post-hardening behavior[3]. For the present study, this cutoff distance is set at 2.0 Å[4].

The interatomic interaction between tip and polycrystalline graphene is described by the long-range van der Waals interactions [5].

In the present MD simulations, we use the hemispherical diamond tip that is allowed to deform together with the circular polycrystalline graphene, as shown in Fig. S1. The tip is prepared by cutting the hemisphere from a bulk diamond sample. The radius of tip is 10 nm. Note that this tip size is similar to that used in recent nanoindentation experiments[6-9]. The tip is first relaxed at 0 K using molecular statics simulations to minimize its total energy. Subsequently the tip is gradually heated to and equilibrated at 300 K. The top 1.0 nm of the tip is held rigidly during simulations of normal loading. The circular polycrystalline graphene is cut from a square polycrystalline graphene. The square polycrystalline graphene sample is generated using the Voronoi tessellation method[10-12]. The sample has a length of 50 nm, width of 50 nm, and contains four randomly oriented grains of various shapes and sizes with an average grain size of 28.2 nm. The grain positions are randomly distributed within the simulation sheet. The created polycrystalline graphene sample is annealed to eliminate low or high-density regions near the grain boundaries (GBs) and junctions. We first anneal the sample at 3000 K for 50 ps after which the sample is quenched to 300 K during a 10 ps run allowing the sample to obtain its equilibrium size (pressure driven to zero)[13]. The edge of the circular polycrystalline graphene with length of 1 nm is held rigidly during simulations of normal loading.

The indentation simulations are performed at 300 K and from the simulations, the normal load vs. indentation depth relation can be obtained. To do so, the tip is driven towards the polycrystalline graphene at speed ranging from 0.25 to 1.0 Å/ps. The normal load is calculated as the average force in the normal direction exerted on the tip by the polycrystalline graphene. The indentation depth is defined as the difference between the lowest point of the tip and the initial

position of the polycrystalline graphene sheet. Periodic boundary conditions are applied in both lateral directions.

Effect of the loading speed

Figure S2 depicts the normal load vs. indentation depth as a function of loading speed for the case of the indenter tip positioned on the center of grain. The changes of the maximum load and indentation depth are not obvious, indicating that the curves of normal load vs. indentation depth are independent of the loading speed in this range from 0.25 to 1.0 Å/ps. In the present work, the loading speed of 0.25 Å/ps is chosen for all the simulations.

Single-crystal graphene indentation

For comparison, the single-crystal graphene indentation is also performed under the same simulation conditions, as shown in Fig. S3(a). The normal load vs. indentation depth (*d*) is plotted in Fig. S3(b). A sequence of snapshots that capture rupture process for single-crystal graphene at different indentation depths are shown in Fig. S3(c). A non-uniform stress distribution is clearly observed around the indenter tip. The stress decreases inversely with distance from the indenter tip. The rupture starts directly from the contact between the tip and the single-crystal graphene due to the high local atomic stresses.

Atomic stress distribution in the polycrystalline graphene

When the indenter tip is positioned at the grain center, it is found that the initial crack starts from a GB rather than grain interior. Figure S4 shows the atomic stress distribution at the indentation depth of 77.2 Å. It is seen that the GB generally has higher atomic stresses. In addition, the strength of GB is weaker than that of the pristine crystalline grain, hence GB is more prone to cracking. It is noted that GB is generally more defected and contains a combination of 5, 7, 8-membered rings, it is less stiff and more compliant, and expected to have a lower load-carrying capacity than grain interior[14].

References

1 Plimpton, S. Fast parallel algorithms for short-range molecular-dynamics. *J. Comput. Phys.* **117**, 1-19 (1995).

2 Stuart, S. J., Tutein, A. B. & Harrison, J. A. A reactive potential for hydrocarbons with intermolecular interactions. *J. Chem. Phys.* **112**, 6472-6486 (2000).

3 Pastewka, L., Pou, P., Perez, R., Gumbsch, P. & Moseler, M. Describing bond-breaking processes by reactive potentials: Importance of an environment-dependent interaction range. *Phys. Rev. B* **78**, 161402 (2008).

4 Zhang, T., Li, X., Kadkhodaei, S. & Gao, H. Flaw insensitive fracture in nanocrystalline graphene. *Nano Lett.* **12**, 4605-4610 (2012).

5 Mo, Y., Turner, K. T. & Szlufarska, I. Friction laws at the nanoscale. *Nature* **457**, 1116-1119 (2009).

6 Lee, C., Wei, X., Kysar, J. W. & Hone, J. Measurement of the elastic properties and intrinsic strength of monolayer graphene. *Science* **321**, 385-388 (2008).

7 Lee, G.-H. *et al.* High-strength chemical-vapor deposited graphene and grain boundaries. *Science* **340**, 1073-1076 (2013).

8 Rasool, H. I., Ophus, C., Klug, W. S., Zettl, A. & Gimzewski, J. K. Measurement of the intrinsic strength of crystalline and polycrystalline graphene. *Nat. Commun.* **4**, 2811 (2013).

9 Ruiz-Vargas, C. S. *et al.* Softened elastic response and unzipping in chemical vapor deposition graphene membranes. *Nano Lett.* **11**, 2259-2263 (2011).

10 Brostow, W., Dussault, J. P. & Fox, B. L. Construction of voronoi polyhedra. *J. Comput. Phys.* **29**, 81-92 (1978).

11 Finney, J. L. Procedure for the construction of voronoi polyhedra. *J. Comput. Phys.* **32**, 137-143 (1979).

12 Tanemura, M., Ogawa, T. & Ogita, N. A new algorithm for 3-dimensional voronoi tessellation. *J. Comput. Phys.* **51**, 191-207 (1983).

13 Kotakoski, J. & Meyer, J. C. Mechanical properties of polycrystalline graphene based on a realistic atomistic model. *Phys. Rev. B* **85**, 195447 (2012).

14 Sha, Z. D., Pei, Q. X., Liu, Z. S., Shenoy, V. B. & Zhang, Y. W. Is the failure of large-area polycrystalline graphene notch sensitive or insensitive? *Carbon* **72**, 200-206 (2014).

Figure Legends

Figure S1: Atomistic model for polycrystalline graphene indentation with the hemispherical diamond tip and the circular polycrystalline graphene, as seen from side, top, and 3D views. The radii of the circular polycrystalline graphene and the hemispherical diamond tip are 25 nm and 10 nm, respectively. The top 1.0 nm of the tip (cyan) and the edge of the polycrystalline graphene with length of 1.0 nm (yellow) are held rigidly during simulations of normal loading.

Figure S2: The normal load vs. indentation depth as a function of loading speed for the case of the indenter tip placed on the center of grain.

Figure S3: The single-crystal graphene indentation. (a) Atomistic model for single-crystal graphene indentation. (b) The normal load vs. indentation depth (d). (c) A sequence of snapshots capturing the rupture process for single-crystal graphene at different indentation depths. The color indicates the von Mises stress. For clarity, the indenter tip is not shown.

Figure S4: (a-b) Atomic stress distribution in the polycrystalline graphene at the indentation depth of 77.2 Å for the case of the indenter tip placed on the center of grain.

Figure S1 SHA et al.

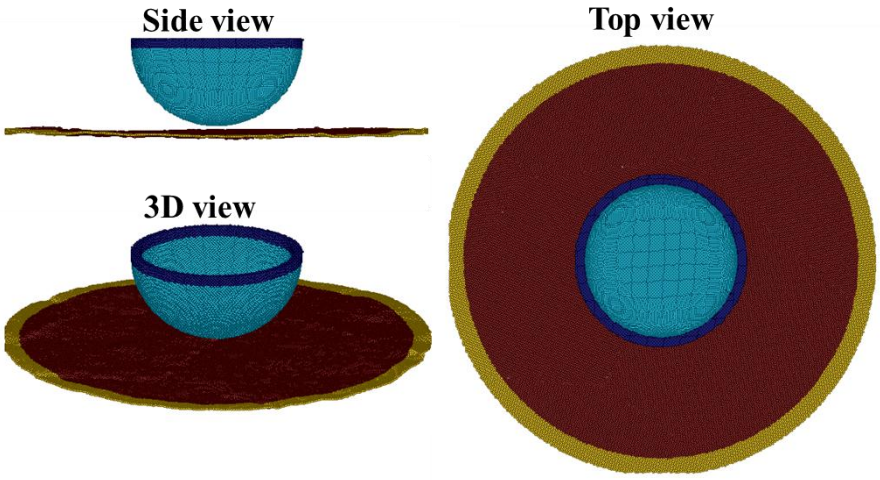

Figure S2 SHA et al.

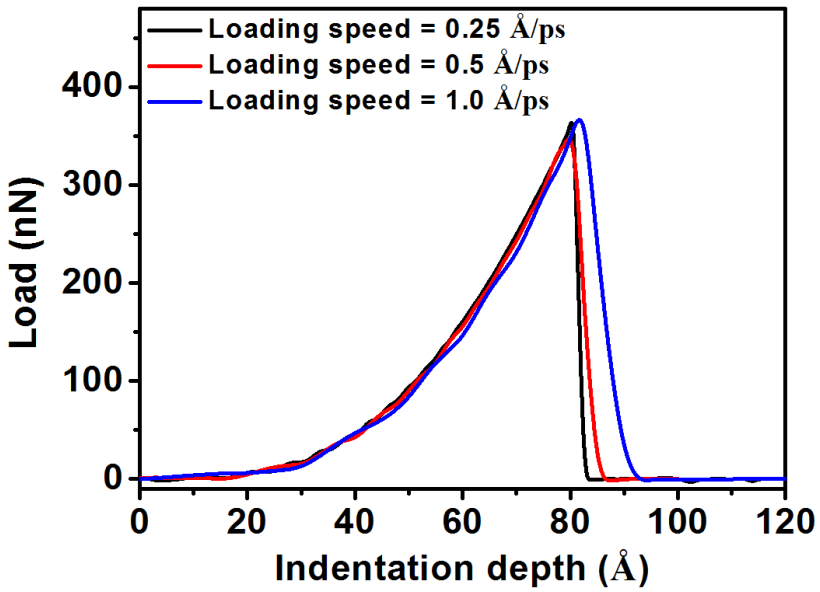

Figure S3 SHA et al.

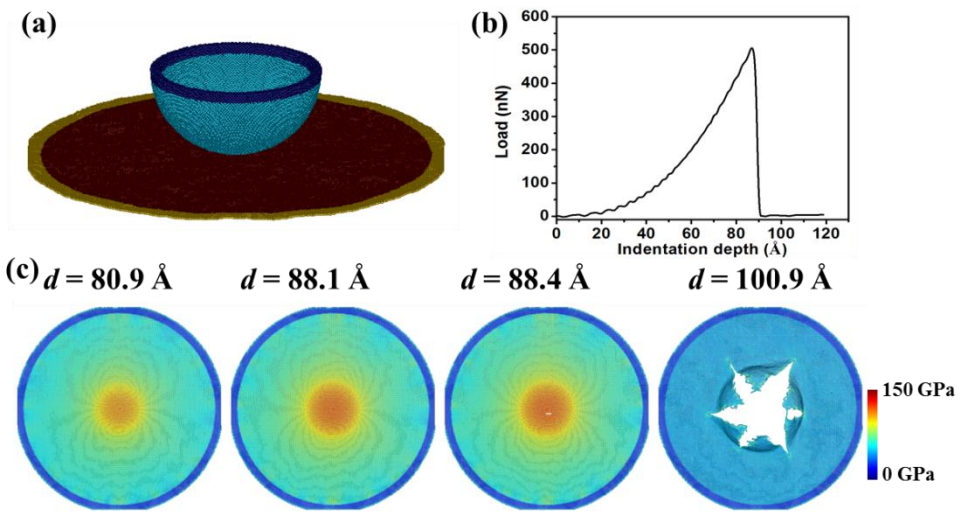

Figure S4 SHA et al.